Prostate Cancer: Accurate Determination of Extracapsular Extension with High-Spatial-Resolution Dynamic Contrast-enhanced and T2-weighted MR Imaging—Initial Results[1]

B. Nicolas Bloch, MD
Edna Furman-Haran, PhD
Thomas H. Helbich, MD
Robert E. Lenkinski, PhD
Hadassa Degani, PhD
Christian Kratzik, MD
Martin Susani, MD
Andrea Haitel, MD
Silvia Jaromi, MD
Long Ngo, PhD
Neil M. Rofsky, MD

Purpose: To prospectively compare the sensitivity and specificity of high-spatial-resolution dynamic contrast material–enhanced magnetic resonance (MR) imaging with those of high-spatial-resolution T2-weighted MR imaging, performed with an endorectal coil (ERC), for assessment of extracapsular extension (ECE) and staging in patients with prostate cancer, with histopathologic findings as reference.

Materials and Methods: The study was approved by the institutional internal review board; a signed informed consent was obtained. MR imaging of the prostate at 1.5 T was performed with combined surface coils and ERCs in 32 patients (mean age, 65 years; range, 42–78 years) before radical prostatectomy. High-spatial-resolution T2-weighted fast spin-echo and high-spatial-resolution dynamic contrast-enhanced three-dimensional gradient-echo images were acquired with gadopentetate dimeglumine. Dynamic contrast-enhanced MR images were analyzed with a computer-generated color-coded scheme. Two experienced readers independently assessed ECE and tumor stage. MR imaging–based staging results were compared with histopathologic results. For the prediction of ECE, sensitivity, specificity, positive predictive value (PPV), and negative predictive value (NPV) were calculated. Staging accuracy was determined with the area under the receiver operating characteristic curve (AUC) by using the Wilcoxon-Mann-Whitney index of diagnostic accuracy.

Results: The mean sensitivity, specificity, PPV, and NPV for assessment of ECE with the combined data sets for both readers were 86%, 95%, 90%, and 93%, respectively. The sensitivity of MR images for determination of ECE was significantly improved for both readers (>25%) with combined data sets compared with T2-weighted MR images alone. The combined data sets had a mean overall staging accuracy for both readers of 95%, as determined with AUC. Staging results for both readers were significantly improved ($P < .05$) with the combined data sets compared with T2-weighted MR images alone.

Conclusion: The combination of high-spatial-resolution dynamic contrast-enhanced MR imaging and T2-weighted MR imaging yields improved assessment of ECE and better results for prostate cancer staging compared with either technique independently.

[1] From the Departments of Radiology (B.N.B., T.H.H., S.J.), Urology (C.K.), and Clinical Pathology (M.S., A.H.), Vienna General Hospital, Medical University of Vienna, Vienna, Austria; Department of Biological Regulation, Weizmann Institute of Science, Rehovot, Israel (E.F., H.D.); and Department of Radiology (B.N.B., R.E.L., N.M.R.), Division of General Medicine and Primary Care (L.N.), Beth Israel Deaconess Medical Center and Harvard Medical School, 330 Brookline Ave, E/Dana 705b, Boston, MA 02215. From the 2002 RSNA Annual Meeting. Received September 8, 2006; revision requested November 9; revision received January 15, 2007; final version accepted March 1. Supported in part by grants of the Jubileumsfonds of the Austrian National Bank, Vienna, Austria (project no. 9570); Medrad, Indianola, Pa; Schering, Berlin, Germany; and Lord David Alliance, CBE, London, England. **Address correspondence to** B.N.B. (e-mail: *nbloch@bidmc.harvard.edu*).

Overall staging of prostate cancer with T2-weighted magnetic resonance (MR) imaging at 1.5 T has shown sensitivity values ranging from 51% to 89% and specificity values ranging from 67% to 87% (1–12). The reported ranges for sensitivity and specificity for determination of extracapsular extension (ECE) are 23%–75% and 84%–97%, respectively (2,3,5,13). These ranges of results have relegated MR imaging to a sparsely used technique for clinical preoperative staging.

For dynamic contrast material–enhanced MR imaging, gadolinium-based contrast media are used, frequently with model-based postprocessing to generate parameters relating to microvascular characteristics of prostate tissue (14–21). Results with such processed dynamic contrast-enhanced MR images have correlated with markers of tumor angiogenesis (22–24). Hence, the additional information gained from dynamic contrast-enhanced MR imaging has been applied to help differentiate benign from malignant tissue, including prostate cancer (25–30).

Researchers in previous studies about dynamic contrast-enhanced MR imaging of the prostate placed an emphasis on high temporal resolution at the expense of spatial resolution, typically by using thick sections and incomplete coverage of the prostate gland. With incomplete sampling of the gland and/or lower spatial resolution, critical features needed for staging may not be visualized, and such a situation leads to potential sacrifice of diagnostic accuracy (8,14,31–33). Thus, the purpose of our study was to prospectively compare the sensitivity and specificity of high-spatial-resolution dynamic contrast-enhanced MR imaging with those of high-spatial-resolution T2-weighted MR imaging, performed with an endorectal coil (ERC), for assessment of ECE and staging in patients with prostate cancer, by using histopathologic findings as the reference standard.

Advance in Knowledge

- The addition of high-spatial-resolution dynamic contrast-enhanced MR imaging substantially improves the accuracy of MR imaging–based staging and facilitates the assessment of extracapsular extension (ECE).

Materials and Methods

This study was partially supported by a grant of the Jubileumsfonds of the Austrian National Bank, Vienna, Austria (project no. 9570). Medrad (Indianola, Pa), Schering (Berlin, Germany), and Lord David Alliance, CBE (London, England), provided financial support (seed grants) for this study. The authors had control of the data and the information submitted for publication. Several authors (B.N.B., H.D., E.F., R.E.L., and N.M.R.) previously were remunerated scientific consultants to 3TP Imaging Sciences, now CAD Sciences (White Plains, NY).

Patients

Between September 2001 and March 2003, 159 men underwent pretherapeutic MR imaging of the prostate for cancer diagnosed by using ultrasonographically guided biopsy. Thirty-two patients (mean age, 65 years; range, 42–78 years) with a mean total prostate-specific antigen level of 9.3 ng/mL (range, 0.99–42.83 ng/mL) and a mean Gleason score of 6 (range, 3–9) were included in the study. In 20% of these patients, the prostate-specific antigen level was less than 5 ng/mL. Patients were selected on the basis of the following entry criteria: *(a)* The patients had biopsy-proved prostate cancer, *(b)* prostatectomy was the treatment plan and was performed within 1 month after MR imaging, *(c)* needle biopsy was performed at least 3 weeks before MR imaging, *(d)* the patients were able to undergo MR imaging with an ERC, *(e)* the patients were able and willing to provide informed consent, and *(f)* the patients had no history of the use of hormonal blockade prior to surgery. Furthermore, 127 patients were excluded from the study because *(a)* they had undergone external-beam radiation therapy ($n = 29$) or brachytherapy ($n = 47$), *(b)* they had undergone prostatectomy but had a history of hormonal treatment prior to MR imaging ($n = 2$), or *(c)* their histopathologic results were not accessible because they had undergone surgery at an outside institution ($n = 49$).

Our study was approved by the institutional internal review board (Ethikkommission) of Vienna General Hospital, Vienna, Austria, and a signed informed consent was obtained from all 32 patients included in the study.

Implications for Patient Care

- The addition of high-spatial-resolution dynamic contrast-enhanced MR imaging substantially enhances the accuracy of MR imaging–based staging and facilitates prediction of ECE.
- This technique has the potential to assist in the selection of patients to undergo the most appropriate therapy for prostate cancer.

MR Imaging Preparations

Patients underwent a cleansing rectal enema (Relaxyl Clyster; Nycomed-Am-

Published online before print
10.1148/radiol.2451061502

Radiology 2007; 245:176–185

Abbreviations:
AUC = area under the receiver operating characteristic curve
ECE = extracapsular extension
ERC = endorectal coil
NPV = negative predictive value
PPV = positive predictive value

Author contributions:
Guarantors of integrity of entire study, B.N.B., T.H.H., R.E.L., N.M.R.; study concepts/study design or data acquisition or data analysis/interpretation, all authors; manuscript drafting or manuscript revision for important intellectual content, all authors; manuscript final version approval, all authors; literature research, B.N.B., E.F., T.H.H., R.E.L., H.D., S.J., L.N.; clinical studies, B.N.B., E.F., T.H.H., C.K., M.S., A.H., S.J.; statistical analysis, S.J., L.N.; and manuscript editing, B.N.B., E.F., T.H.H., H.D., C.K., L.N., N.M.R.

See Materials and Methods for pertinent disclosures.

ersham, Linz, Austria) 1–3 hours before the MR imaging examination. Lubrication and local anesthesia of the anal region with topical application of 2% lidocaine gel (Xylocaine; AstraZeneca, Wedel, Germany) immediately preceded the placement of the ERC. An antiperistaltic agent, 0.5 mg glucagon (Glucagen; Novo Nordisc, Bagsvaerd, Denmark), was administered intravenously just before the MR imaging examinations, and an additional 0.5 mg was administered immediately preceding the dynamic contrast-enhanced MR acquisitions.

MR Imaging Protocol

All of the examinations were performed with a 1.5-T imaging unit and a pelvic phased-array surface coil (Magnetom Vision; Siemens Medical Solutions, Erlangen, Germany) combined with a disposable prostate ERC (MRinnervu; Medrad, Pittsburgh, Pa). Images were corrected for the reception profile of the ERC and the pelvic phased-array coil (34).

Multiplanar localizer images were obtained first. Then, transverse dual-echo T2-weighted fast spin-echo images were acquired from below the apex of the prostate to above the seminal vesicles with a voxel size of 1.68 mm^3 ($0.89 \times 0.63 \times 3$ mm) in 10 minutes 48 seconds (Table 1).

High-spatial-resolution dynamic contrast-enhanced MR imaging was performed with application of a fast three-dimensional T1-weighted spoiled gradient-echo sequence with a voxel size of 1.79 mm^3 ($0.95 \times 0.63 \times 3$ mm). Seven three-dimensional data sets, two before and five after contrast agent administration, were acquired with a 1 minute 35 second temporal resolution and a total duration of 11 minutes 8 seconds. The MR contrast agent, gadopentetate dimeglumine (Magnevist; Schering, Berlin, Germany), was injected as a bolus at a dose of 0.1 mmol per kilogram of body weight. For this purpose, an automated injection system (Spectris Solaris EP; Medrad, Pittsburgh, Pa) was used at a flow rate of 4 mL/sec at 5–7 seconds before the end of the second acquisition before contrast agent administration. Immediately after, a 20-mL saline flush was administered at a rate of 4 mL/sec.

MR Image Interpretation

The images were interpreted independently by two radiologists, who were blinded to all patient information other than knowing that each patient had biopsy-proved prostate cancer. Reader 1 (B.N.B.) had 4 years of MR imaging experience and had read approximately 500 T2-weighted and dynamic contrast-enhanced MR images from prostate examinations during that time. Reader 2 (N.M.R.) had 15 years of MR imaging experience and had read approximately 1300 images from prostate examinations during that time, and 100 of them included dynamic contrast-enhanced MR images of the prostate.

A focal hypointense mass in the peripheral zone on T2-weighted MR images without corresponding hyperintense signal on nonenhanced T1-weighted MR images was considered to represent tumor. Criteria for determination of ECE of a mass on T2-weighted MR images included at least one of the following: disruption of the prostatic capsule, extension into the periprostatic fat contiguous with low-signal-intensity tumor in the gland, broad contact with the capsule (>12 mm), irregular capsular bulge, obliteration of the rectoprostatic angle, or asymmetry or involvement of the neurovascular bundle (35,36). Features of seminal vesicle infiltration were focal low signal intensity in one or both sides, with low signal intensity in the base of the prostate or tubular wall thickening combined with tumor mass in the base of the prostate (37,38).

Dynamic contrast-enhanced images were processed at pixel resolution by using the three-time-point model (28) to analyze the time evolution of contrast enhancement. The results were translated into a color-coded scheme, as previously published (Fig 1) (25,28).

The processed color-coded images, overlaid on the original T1-weighted gray-scale images, were analyzed as follows: Masslike nodular or geographic clusters of bright red pixels in the peripheral zone with more than 4 mm in

Table 1

Imaging Parameters

Parameter	T2-weighted MR Imaging	Dynamic MR Imaging
Repetition time msec/echo time msec	4000/83, 165	8.1/4
Flip angle (degrees)	90	18
Echo train length	9	1
Phase oversampling	100	100
Section thickness (mm)	3	3
Intersection gap	None	None
Frequency-encoding steps	256	256
Phase-encoding steps	180	168
Field of view (cm)	16	16
Voxel size (mm^3)	1.68	1.79
Phase encoding	Left to right	Left to right
Excitation order	Interleaved	Linear
Measurements	2	7
Time gap	. . .	None
No. of signals acquired	2	1
No. of sections	28 (14 sections × 2 measurements)	32
Image time	5 min 24 sec	1 min 35 sec
Total image time	10 min 48 sec	11 min 8 sec

Note.—T2-weighted MR imaging = two-dimensional T2-weighted fast spin-echo MR imaging, dynamic MR imaging = three-dimensional T1-weighted spoiled gradient-echo dynamic contrast-enhanced MR imaging.

maximal diameter were noted as probable or definite cancer (with the scoring system mentioned later). Tubular clusters in a linear orientation were considered as vessels. In the central gland, clusters of bright red pixels more than 6 mm in diameter—which also showed an asymmetric geographic distribution pattern in comparison with the contralateral side, were ill-defined, or had contact with a suspicious area in the peripheral zone—were considered as probable cancer. Well-defined, approximately symmetric nodularlike lesions in the central gland were considered as benign prostatic hyperplasia. Extracapsular bright red pixel clusters, larger than 3 mm in diameter, which were not tubular (blood vessels), were considered as suspicious or definite ECE.

Combined Analysis of T2-weighted MR Images and Dynamic Contrast-enhanced MR Images

After separate evaluation and classification of T2-weighted MR images and color-coded dynamic contrast-enhanced MR images, each reader independently reviewed both images in combination. To avoid a sequential reading bias, each reader started with T2-weighted MR images for 16 patients; for the other 16 patients, dynamic contrast-enhanced MR images were read first. After one image was assigned a score, evaluation of the other followed immediately, and a distinct score for the combined T2-weighted MR image and dynamic contrast-enhanced MR image readings was generated.

Assignment of Scores to the Data

The likelihood of the presence of cancer, seminal vesicle infiltration, and ECE was assigned a score separately by using a five-point rating scale (34): score 1, not present; score 2, probably not present; score 3, possibly present; score 4, probably present; and score 5, definitely present. This scale was applied for the T2-weighted MR images, the dynamic contrast-enhanced MR images, and the combined data sets, and scores were assigned on separate evaluation templates. The results were then dichotomized so that cancer, ECE, or seminal vesicle infiltration was diagnosed for images with scores of 4 and 5 (probable and definite) and was not diagnosed for images with scores of 1–3 (34). Finally, scores for intra- and extraglandular disease were translated into an MR imaging–based TNM stage by using the TNM stage in the 1997 publication of the American Joint Committee on Cancer (39) (Table 2).

Histopathologic Evaluation Results as Reference Standard

Whole-mount histopathologic preparation of the excised prostate gland was performed in 15 patients. The specimen was fixed in 10% buffered formaldehyde, embedded in paraffin, sectioned (3–4-mm thickness) consecutively in planes closely paralleling the MR images, and stained with hematoxylin-eosin.

All of the specimens were classified according to stage and grade by one pathologist (A.H.), who had 15 years of experience in prostate histopathologic examination and was unaware of the MR imaging results. This classification was performed by using the 1997 TNM staging classification and the Gleason score. Areas of carcinoma were circumscribed by a solid red line; areas of prostatic intraepithelial neoplasia were marked by a black dotted line. The whole-mount histopathologic slices were compared

Figure 1

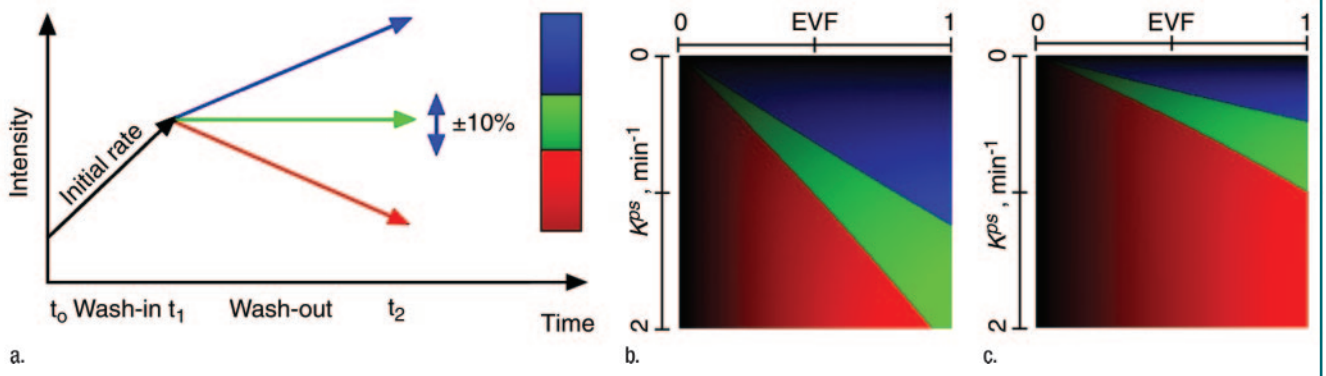

Figure 1: **(a)** Color-coding scheme. The pattern at the washout phase is coded according to color: red for clearance, green for steady state, and blue for continued entrance. The initial change in signal intensity of the wash-in phase (initial rate) is coded according to color intensity: 255 color intensities for each color hue. **(b)** Calibration map constructed with the three times: t_0, at 0 minutes (before contrast agent administration); t_1, at 0.8 minutes; and t_2, at 7.1 minutes (after contrast agent administration). This selection of times yielded the optimal color resolution for the various microvascular permeability *(K^{ps})* and extracellular volume fraction *(EVF)* values. **(c)** Calibration map constructed with the three times: t_0, at 0 minutes (before contrast agent administration); t_1, at 2.4 minutes; and t_2, at 7.1 minutes (after contrast agent administration). For most microvascular permeability and extracellular volume fraction values, the color is red, and, therefore, color resolution for the various microvascular permeability and extracellular volume fraction values is lost. For calculation of the map, a fast gradient-echo sequence (4/8.1; flip angle, 18°) was used. Other parameters used in the calculation were previously published (28). On the basis of an initial learning curve, we used the first and last, as well as the second and last, contrast-enhanced acquisition parametric sets for evaluation. The second and last parametric sets were used when clusters of green and dark red were seen on the first and last parametric sets to search for a transition to bright red.

by means of visual inspection with the corresponding T2-weighted MR images and the dynamic contrast-enhanced MR imaging maps by the pathologist (A.H.) and one radiologist (B.N.B.) in consensus.

In the remaining 17 patients, step-section sextant histopathologic analysis was performed, with the tissue preparation otherwise identical to that of the whole-mount processing. The overall pathology report and histopathologic finding–based TNM stage were compared with the corresponding MR imaging results and MR imaging–based TNM stages by two individuals (S.J. and B.N.B.).

Table 2

Tumor Staging Categories

Tumor Stage	Description
T1	Tumor is clinically unapparent, not palpable, or not visible with imaging
T2	Tumor is confined within prostate
T2a	Tumor involves one lobe
T2b	Tumor involves both lobes
T3	Tumor extends through prostatic capsule or seminal vesicles
T3a	Tumor has unilateral or bilateral ECE
T3b	Tumor invades seminal vesicles
T4	Tumor invades other structures, such as the urinary bladder, internal sphincter, and rectal wall

Note.—The tumor stage categories are based on data on TNM stage in the 1997 publication of the American Joint Committee on Cancer (39).

Statistical Analysis

The ECE analysis was performed by first grouping the stages into two categories (T3a and T3b vs T2a and T2b). ECE is defined as a stage of T3a or T3b. Because ECE is binary, the diagnostic accuracy measures used were sensitivity, specificity, positive predictive value (PPV), and negative predictive value (NPV). These estimates, along with the corresponding 95% confidence intervals, were calculated on the basis of the algorithm provided by Zhou et al (40). In addition, patients with T3b disease were analyzed separately to address this clinically relevant cohort.

The 95% confidence intervals were computed by using the score confidence interval (41,42) because most of these estimates were close to a score of 1. The calculation of the PPV and NPV was performed by using the study population prevalence of 34% and a screening population prevalence estimate of 3.2% (43). We set the type I error rate at 5%; however, we are aware that the sample size in this study is small, especially when the sample of 32 subjects was stratified (16 in each group) to examine the effect of the order in which the methods were performed. Therefore, it is likely that, for a particular comparison between the two methods, although a statistically significant difference may exist, we do not have sufficient study power.

To compare the diagnostic accuracy values of the three modalities (dynamic contrast-enhanced MR imaging, T2-weighted MR imaging, and the combination of both methods), we computed the area under the receiver operating characteristic curve (AUC) for each method. The AUC is a standard measure of diagnostic accuracy that takes into account both the sensitivity and specificity of the test method (44). Four stages (T2a, T2b, T3a, T3b) were used to calculate the AUC by using the Wilcoxon-Mann-Whitney index of diagnostic accuracy (45). The 95% confidence interval was also provided. The staging analysis was performed separately for each of the two readers to observe between-reader variability.

The staging analysis was also performed for two groups of subjects on the basis of the order in which the methods were performed (dynamic contrast-enhanced MR images read first or T2-weighted MR images read first). In one group with 16 subjects, dynamic contrast-enhanced MR images were read first, and in the other

Figure 2

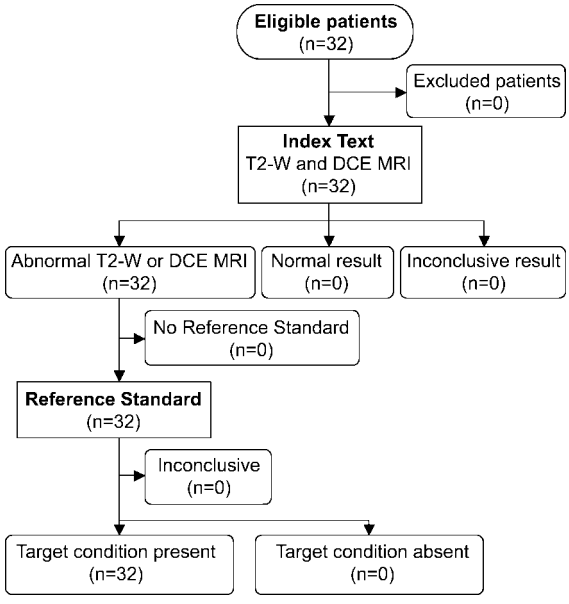

Figure 2: Flowchart of the study profile, which was based on recommended standards for reporting diagnostic accuracy (47). *DCE* = dynamic contrast enhanced.

group of 16 subjects, T2-weighted MR images were read first. All statistical analyses were performed by using software (SAS, 2000; SAS Institute, Cary, NC) (46).

Results

No patients were excluded (Fig 2). Both readers showed a tendency to improve their results for determination of ECE with the use of dynamic contrast-enhanced MR images (Tables 3–5). There were readings in which errors occurred when periprostatic blood vessels were misinterpreted as ECE (reader 1, twice; reader 2, once). These data resulted in misclassification of T2b tumors as T3a disease with the use of dynamic contrast-enhanced MR images alone. For these readings, use of the combined data sets led to correction of this misclassification to the true pathologic tumor stage in two of three patients (reader 1, once; reader 2, once) (Fig 3).

Prediction of Stage T3a and T3b ECE

The sensitivity for determination of ECE, with use of the combined data sets, was 91% for reader 1 and 82% for reader 2 (Table 4). For both readers, sensitivity for determination of ECE, with T2-weighted MR images, could be improved by more than 25% after the addition of dynamic contrast-enhanced MR images, although the difference was not statistically significant ($P = .083$ for both readers). For both readers, the specificity for the combined data sets was the same (95%). For reader 1, the specificity improved by 9% when T2-weighted MR images and dynamic contrast-enhanced MR images were combined; for reader 2, the specificity improved by 4%, but this improvement was not statistically significant ($P = .157$ and .564, respectively).

For readers 1 and 2, the PPV value achieved by using the combined data sets improved by 21% and 15%, respectively, compared with the PPV achieved by using T2-weighted MR images alone. These values were calculated by using the 34% (11 of 32) ECE prevalence of our study (Table 4).

The NPV for readers 1 and 2 was as follows: The NPV for the combined data sets was greater than that for dynamic contrast-enhanced MR images alone and greater than that for T2-weighted MR images alone, by using the 34% ECE prevalence of our study (Table 4). The use of combined data sets, compared with T2-weighted MR images alone, improved the NPVs by 13% and 12% for reader 1 and reader 2, respectively.

Adjustments to the PPV and NPV, by using the estimated 3.2% prevalence of ECE in a screening population, are also shown (Table 4) (43).

Staging Results

Both readers showed improvement in TNM staging (Table 5) when the combined data sets, as compared with the use of data from each strategy independently, were used. Both readers showed

Table 3

Assessment of ECE and Seminal Vesicle Infiltration with T2-weighted MR Images, Dynamic MR Images, and Combined Data Sets

	Reader 1			Reader 2		
Correct Assessment	T2-weighted MR Images	Dynamic MR Images	Combined Data Sets	T2-weighted MR Images	Dynamic MR Images	Combined Data Sets
ECE	64 (7/11)	91 (10/11)	91 (10/11)	55 (6/11)	82 (9/11)	82 (9/11)
Seminal vesicle infiltration	100 (5/5)	100 (5/5)	100 (5/5)	100 (5/5)	100 (5/5)	100 (5/5)

Note.—Data are percentages. Numbers in parentheses were used to calculate the percentages. Sequences are defined in Table 1.

Table 4

Diagnostic Accuracy for Assessment of ECE Adjusted to the Prevalence of Disease in the Study Population and in the Population at Large

	Reader 1			Reader 2		
Statistic	T2-weighted MR Images	Dynamic MR Images	Combined Data Sets	T2-weighted MR Images	Dynamic MR Images	Combined Data Sets
Sensitivity	64 (35, 85)	91 (62, 98)	91 (62, 98)	54 (28, 79)	82 (52, 95)	82 (52, 95)
Specificity	86 (65, 95)	86 (65, 95)	95 (77, 99)	91 (71, 97)	86 (65, 95)	95 (77, 99)
PPV	70 (40, 89)	77 (50, 92)	91 (62, 98)	75 (41, 93)	75 (47, 91)	90 (60, 98)
NPV	82 (62, 93)	95 (75, 99)	95 (77, 99)	79 (60, 91)	90 (70, 97)	91 (72, 98)
Adjusted PPV*	13 (3, 44)	17 (5, 44)	39 (17, 67)	16 (3, 50)	16 (4, 44)	36 (14, 66)
Adjusted NPV*	99 (83, 100)	100 (83, 100)	100 (84, 100)	98 (84, 100)	99 (83, 100)	99 (84, 100)

Note.—Data are percentages, which have been rounded. Numbers in parentheses are 95% confidence intervals expressed as percentages. Sequences are defined in Table 1.
* Data were adjusted to the prevalence of disease in the study population (34% prevalence) and in the population at large (3.2% prevalence).

Table 5

Percentage of Correct Staging, Understaging, and Overstaging and Staging Accuracy in 32 Patients: Comparison of T2-weighted MR Images, Dynamic MR Images, and Combined Data Sets

	Reader 1			Reader 2		
Staging	T2-weighted MR Images	Dynamic MR Images	Combined Data Sets	T2-weighted MR Images	Dynamic MR Images	Combined Data Sets
Correct	72 ($n = 23$)	84 ($n = 27$)	91 ($n = 29$)	72 ($n = 23$)	81 ($n = 26$)	88 ($n = 28$)
Understaging	19 ($n = 6$)	3 ($n = 1$)	3 ($n = 1$)	19 ($n = 6$)	9 ($n = 3$)	9 ($n = 3$)
Overstaging	9 ($n = 3$)	12 ($n = 4$)	6 ($n = 2$)	9 ($n = 3$)	9 ($n = 3$)	3 ($n = 1$)
AUC*	84 (75, 94)	92 (84, 100)	95 (88, 100)	86 (77, 95)	94 (88, 99)	96 (92, 100)†

Note.—All data are percentages. Sequences are defined in Table 1.

* Numbers in parentheses are 95% confidence intervals.

† Improvement versus T2-weighted MR images for reader 2 ($P = .042$).

a tendency to understage disease when T2-weighted MR images (Table 5 and Fig 4) were used, whereas with dynamic contrast-enhanced MR images, both readers showed a tendency to overstage disease. There was no statistically significant difference with respect to the effect of the viewing order on the determination of ECE or the staging results.

Diagnostic Accuracy Analysis of Staging by Using AUC

By using the combined data sets, the diagnostic accuracy (AUC) was 95% and 96%, respectively, for reader 1 and reader 2 (Table 5). For both readers, the AUC values were as follows: Values for combined data sets were greater than those for dynamic contrast-enhanced MR images alone and for T2-weighted MR images alone. The AUC for TNM staging that was based on the combined data sets exceeded that which was based on only T2-weighted MR images by 10% for reader 2 and indicated a statistically significant improvement ($P = .042$) (Table 5).

Figure 3

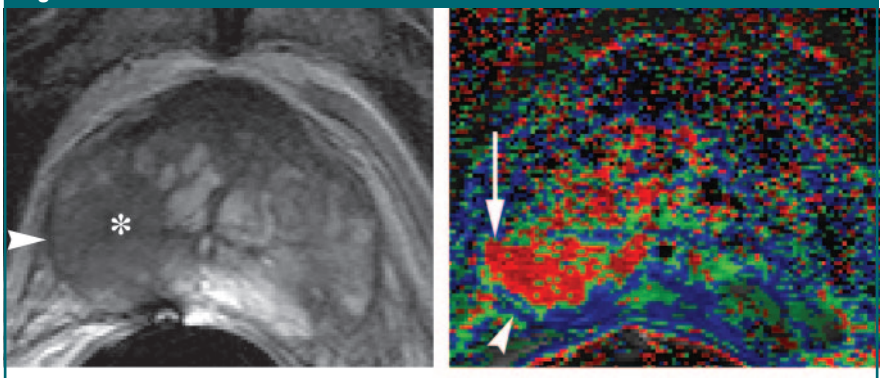

a. b.

Figure 3: Corresponding T2-weighted MR image and dynamic contrast-enhanced MR image–based color-coded image. **(a)** Transverse 3-mm-thick dual T2-weighted fast spin-echo MR image (4000/83 [effective]) of the middle third of the prostate. Large cancer area is in the right peripheral zone and adjacent central gland (*). Capsule (arrowhead) is clearly distinguishable and well defined. Both readers staged this cancer as T2b on the basis of T2-weighted MR imaging findings. **(b)** Color-coded 3-mm-thick dynamic contrast-enhanced three-dimensional gradient-echo MR image (8.1/4) corresponding to **a.** Capsule (arrow) shows irregularity, in contrast to well-defined capsule (arrowhead). Both readers diagnosed ECE. Use of combined data sets led to a final combined MR imaging–based stage of T2b (well-defined capsule on T2-weighted MR images overruled the dynamic contrast-enhanced MR image findings). This stage was proved correct at histopathologic evaluation (pT2b).

Discussion

Findings in studies in which MR imaging was used for prostate cancer staging and/or prediction of ECE have yielded a range of values for accuracy (56%–88%), sensitivity (51%–89%), and specificity (68%–87%) (2,48–50). Differences in reader expertise, MR equipment, and study protocols each might influence this variability (51–56).

The T2-weighted MR imaging accuracy achieved by both readers in this study is at the high end but within the range of previously published staging results with T2-weighted MR imaging. The combination of T2-weighted MR imaging and high-spatial-resolution dynamic contrast-enhanced MR imaging data showed a positive synergistic effect, yielding the highest staging accuracy of the three approaches and exceeding previously published results achieved with 1.5-T MR imaging.

We observed some tumors on dynamic contrast-enhanced MR images that were unapparent on T2-weighted MR images, and this difference augmented sensitivity. Furthermore, observed boosts in specificity from dynamic contrast-enhanced MR images may have resulted from clarification of benign sources of low-signal-intensity foci that mimic cancer, such as postbiopsy hemorrhage, prostatitis, calcification, and treatment effects, that were observed on T2-weighted MR images

(2,51,54–56). On the other hand, the high detail and definition of T2-weighted MR images can help refine the dynamic contrast-enhanced MR imaging analysis in which color-coded pixels may interfere with anatomic landmarks.

Our choice to acquire high-spatial-resolution images at a temporal resolution of 95 seconds, influenced by previous breast imaging studies (57), is a departure from prior high-temporal-resolution dynamic contrast-enhanced MR imaging studies. Highly temporally resolved dynamic contrast-enhanced MR imaging studies necessitated tradeoffs in spatial resolution and/or anatomic coverage of the gland. Thus, critical features needed for MR imaging–based staging may have been incompletely visualized or characterized, and such a deficiency contributed to the results that have been reported (8,14,31,33,58,59).

The voxel size of 1.79 mm^3 that we used at dynamic contrast-enhanced MR imaging was applied with complete coverage of the gland and the seminal vesicles. In comparison, the voxel size for dynamic contrast-enhanced MR imaging with the highest spatial resolution that we could find in the literature was 6 mm^3 ($6 \times 1 \times 1$ mm) (32).

With our technique, clear and distinct signal intensity changes for the dynamic contrast-enhanced MR imaging analysis were spatially and temporally sufficient according to the concepts of Degani et al (28). By applying a linear-ordered gradient-echo sequence to the first contrast-enhanced data set and having its center of k-space obtained at 47.5 seconds after contrast agent injection, our time is only a few seconds beyond the previously determined average contrast enhancement peak of cancerous prostatic tissue (31,60). In future studies, it may be interesting to assess the value of alternative methods for presenting dynamic contrast-enhanced MR imaging data and their influence on diagnostic accuracy with respect to reader experience.

Both readers achieved sensitivity, specificity, PPV, and NPV at the high end or at values greater than previously published data by using the combined data sets for the evaluation of the preoperative prediction of ECE (2,3,5,13,36,61). Prevalence-adjusted data are important when one considers prostate MR imaging as part of a screening protocol for staging. Although our adjusted data showed a preserved NPV for determination of ECE at 99% for both readers with the use of combined data sets, the PPV diminished to less than 40% in the population at large from 90% in our study population. The high NPV is encouraging for a screening application, but the current high cost of MR imaging makes such an application impractical.

The recent availability of high-spatial-resolution T2-weighted MR imaging at 3 T with an ERC offers new possibilities (62,63). In a recent report, Futterer et al (59) showed impressive staging results by using T2-weighted MR imaging at 3 T that are in the range of our results. The potential added value of dynamic contrast-enhanced MR imaging at 3 T needs to be explored. However, at the time of this writing, 3 T MR imaging with an ERC is limited to a few centers.

Our study had recognized limitations. The relatively small number of patients may have affected the statistical relevance of the results. In addition, histopathologic specimens were not processed uniformly with whole-mount preparation.

The combined approach of high-spatial-resolution dynamic contrast-enhanced MR imaging and high-spatial-resolution T2-weighted MR imaging at

Figure 4

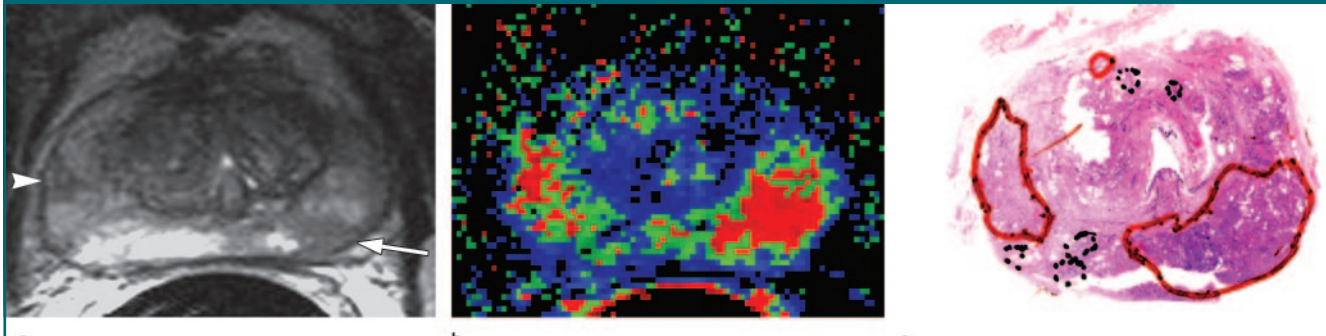

Figure 4: T2-weighted MR image and dynamic contrast-enhanced MR imaging–based color-coded image in correlation with whole-mount histopathologic specimen. **(a)** Transverse 3-mm-thick T2-weighted fast spin-echo MR image (4000/83) of the middle third of the prostate. In this study, the two readers identified a highly suspicious hypointense area (score of 4) in the left peripheral zone (arrow) on the T2-weighted MR image. On the right side, the hypointense triangularly shaped signal intensity alteration in the lateral peripheral zone (arrowhead) was noted by one reader as possible cancer (score of 3), and this observation resulted in a final T2-weighted MR imaging–based stage of T2a. The second reader rated the triangular lesion as probably cancer (score of 4) and the lesion on the left side as definitely cancer (score of 5), with a final T2-weighted MR imaging–based stage of T2b. **(b)** Color-coded 3-mm-thick dynamic contrast-enhanced three-dimensional gradient-echo MR image (8.1/4) shows bilateral cancer (bright red area), yielding a dynamic contrast-enhanced MR imaging–based stage of T2b. The results obtained from the color images yielded a combined MR imaging stage of T2b for both readers. **(c)** Whole-mount histopathologic specimen for which the stage was proved to be T2b. A small cancer focus is close to the fibromuscular band in the anterior portion of the gland (circled in red), and small foci of prostate intraepithelial neoplasia (circled with black dotted line) are evident.

1.5 T with a TNM staging accuracy of 95% offers an alternative to conventional prostate cancer staging that is based on results of standard clinical evaluations or findings on T2-weighted MR images alone. The addition of high-spatial-resolution dynamic contrast-enhanced MR imaging substantially enhances the accuracy of MR imaging–based staging and facilitates prediction of ECE.

Acknowledgments: The authors thank Monika Kaderk, RT, Elisabeth Fuchs, RT, and Sonia Diem, RT, for their support and participation in this study. We also thank Dov Grobgeld, PhD, for developing the software for analysis of dynamic contrast-enhanced MR images. Furthermore, we thank Gerhard Lechner, MD, for his support and encouragement. Finally, we acknowledge Lois Gilden for revision of the several versions of the manuscript.

References

1. Yu KK, Hricak H. Imaging prostate cancer. Radiol Clin North Am 2000;38:59–85, viii.
2. Jager GJ, Ruijter ET, van de Kaa CA, et al. Local staging of prostate cancer with endorectal MR imaging: correlation with histopathology. AJR Am J Roentgenol 1996;166:845–852.
3. Ikonen S, Karkkainen P, Kivisaari L, et al. Magnetic resonance imaging of clinically localized prostatic cancer. J Urol 1998;159:915–919.
4. Chelsky MJ, Schnall MD, Seidmon EJ, Pollack HM. Use of endorectal surface coil magnetic resonance imaging for local staging of prostate cancer. J Urol 1993;150:391–395.
5. Perrotti M, Kaufman RP Jr, Jennings TA, et al. Endo-rectal coil magnetic resonance imaging in clinically localized prostate cancer: is it accurate? J Urol 1996;156:106–109.
6. Quinn SF, Franzini DA, Demlow TA, et al. MR imaging of prostate cancer with an endorectal surface coil technique: correlation with whole-mount specimens. Radiology 1994;190:323–327.
7. Brown G, Macvicar DA, Ayton V, Husband JE. The role of intravenous contrast enhancement in magnetic resonance imaging of prostatic carcinoma. Clin Radiol 1995;50:601–606.
8. Jager GJ, Ruijter ET, van de Kaa CA, et al. Dynamic TurboFLASH subtraction technique for contrast-enhanced MR imaging of the prostate: correlation with histopathologic results. Radiology 1997;203:645–652.
9. Hricak H. Noninvasive imaging for staging of prostate cancer: magnetic resonance imaging, computed tomography, and ultrasound. NCI Monogr 1988;7:31–35.
10. Hricak H, Dooms GC, Jeffrey RB, et al. Prostatic carcinoma: staging by clinical assessment, CT, and MR imaging. Radiology 1987;162:331–336.
11. Hricak H, White S, Vigneron D, et al. Carcinoma of the prostate gland: MR imaging with pelvic phased-array coils versus integrated endorectal–pelvic phased-array coils. Radiology 1994;193:703–709.
12. D'Amico AV, Whittington R, Malkowicz SB, et al. Critical analysis of the ability of the endorectal coil magnetic resonance imaging scan to predict pathologic stage, margin status, and postoperative prostate-specific antigen failure in patients with clinically organ-confined prostate cancer. J Clin Oncol 1996;14:1770–1777.
13. Sanchez-Chapado M, Angulo JC, Ibarburen C, et al. Comparison of digital rectal examination, transrectal ultrasonography, and multicoil magnetic resonance imaging for preoperative evaluation of prostate cancer. Eur Urol 1997;32:140–149.
14. Padhani AR, Gapinski CJ, Macvicar DA, et al. Dynamic contrast enhanced MRI of prostate cancer: correlation with morphology and tumour stage, histological grade and PSA. Clin Radiol 2000;55:99–109.
15. Padhani AR. Dynamic contrast-enhanced MRI in clinical oncology: current status and future directions. J Magn Reson Imaging 2002;16:407–422.
16. Helbich TH, Gossman A, Mareski PA, et al. A new polysaccharide macromolecular contrast agent for MR imaging: biodistribution and imaging characteristics. J Magn Reson Imaging 2000;11:694–701.
17. Gossmann A, Okuhata Y, Shames DM, et al. Prostate cancer tumor grade differentiation with dynamic contrast-enhanced MR imaging in the rat: comparison of macromolecular and small-molecular contrast media—preliminary experience. Radiology 1999;213:265–272.
18. Oyen RH. Dynamic contrast-enhanced MRI of the prostate: is this the way to proceed for characterization of prostatic carcinoma? Eur Radiol 2003;13:921–924.
19. Buckley DL, Roberts C, Parker GJ, Logue JP, Hutchinson CE. Prostate cancer: evaluation of vascular characteristics with dynamic contrast-enhanced T1-weighted MR imaging—initial experience. Radiology 2004;233:709–715.
20. Schlemmer HP, Merkle J, Grobholz R, et al. Can pre-operative contrast-enhanced dynamic MR imaging for prostate cancer predict microvessel density in prostatectomy specimens? Eur Radiol 2004;14:309–317.
21. Preziosi P, Orlacchio A, Di Giambattista G, et al. Enhancement patterns of prostate cancer in dynamic MRI. Eur Radiol 2003;13:925–930.
22. Folkman J, Beckner K. Angiogenesis imaging. Acad Radiol 2000;7:783–785.
23. Li WW. Tumor angiogenesis: molecular pathology, therapeutic targeting, and imaging. Acad Radiol 2000;7:800–811.
24. Folkman J. Angiogenesis in cancer, vascular, rheumatoid and other disease. Nat Med 1995;1:27–31.
25. Furman-Haran E, Degani H. Parametric analysis of breast MRI. J Comput Assist Tomogr 2002;26:376–386.
26. Taylor JS, Tofts PS, Port R, et al. MR imaging of tumor microcirculation: promise for the new millennium. J Magn Reson Imaging 1999;10:903–907.
27. Passe TJ, Bluemke DA, Siegelman SS. Tumor angiogenesis: tutorial on implications for imaging. Radiology 1997;203:593–600.
28. Degani H, Gusis V, Weinstein D, Fields S, Strano S. Mapping pathophysiological features of breast tumors by MRI at high spatial resolution. Nat Med 1997;3:780–782.
29. Huch Boni RA, Boner JA, Lutolf UM, Trinkler F, Pestalozzi DM, Krestin GP. Contrast-enhanced endorectal coil MRI in local staging of prostate carcinoma. J Comput Assist Tomogr 1995;19:232–237.
30. Huisman HJ, Engelbrecht MR, Barentsz JO. Accurate estimation of pharmacokinetic contrast-enhanced dynamic MRI parameters of the prostate. J Magn Reson Imaging 2001;13:607–614.
31. Engelbrecht MR, Huisman HJ, Laheij RJ, et al. Discrimination of prostate cancer from normal peripheral zone and central gland tissue by using dynamic contrast-enhanced MR imaging. Radiology 2003;229:248–254.
32. Ogura K, Maekawa S, Okubo K, et al. Dynamic endorectal magnetic resonance imaging for local staging and detection of neurovascular bundle involvement of prostate cancer: correlation with histopathologic results. Urology 2001;57:721–726.
33. Ito H, Kamoi K, Yokoyama K, Yamada K, Nishimura T. Visualization of prostate cancer using dynamic contrast-enhanced MRI: comparison with transrectal power Doppler ultrasound. Br J Radiol 2003;76:617–624.
34. Scheidler J, Hricak H, Vigneron DB, et al. Prostate cancer: localization with three-dimensional proton MR spectroscopic imag-

ing—clinicopathologic study. Radiology 1999; 213:473–480.

35. Yu KK, Hricak H, Alagappan R, Chernoff DM, Bacchetti P, Zaloudek CJ. Detection of extracapsular extension of prostate carcinoma with endorectal and phased-array coil MR imaging: multivariate feature analysis. Radiology 1997;202:697–702.

36. Yu KK, Scheidler J, Hricak H, et al. Prostate cancer: prediction of extracapsular extension with endorectal MR imaging and three-dimensional proton MR spectroscopic imaging. Radiology 1999;213:481–488.

37. Cornud F, Flam T, Chauveinc L, et al. Extraprostatic spread of clinically localized prostate cancer: factors predictive of pT3 tumor and of positive endorectal MR imaging examination results. Radiology 2002;224:203–210.

38. Song SK, Qu Z, Garabedian EM, Gordon JI, Milbrandt J, Ackerman JJ. Improved magnetic resonance imaging detection of prostate cancer in a transgenic mouse model. Cancer Res 2002;62:1555–1558.

39. American Joint Committee on Cancer. Prostate. In: AJCC cancer staging manual. 5th ed. Philadelphia, Pa: Lippincott-Raven, 1997; 219–224.

40. Zhou XH, Obuchowski NA, McClish DK. Statistical methods in diagnostic medicine. New York, NY: Wiley, 2002.

41. Agresti A, Coull BA. Order-restricted tests for stratified comparisons of binomial proportions. Biometrics 1996;52:1103–1111.

42. Coull BA, Agresti A. The use of mixed logit models to reflect heterogeneity in capture-recapture studies. Biometrics 1999;55:294–301.

43. U.S. Congress Office of Technology Assessment. Cost and effectiveness of prostate cancer screening in elderly men. Washington, DC: U.S. Government Printing Office, 1995.

44. Obuchowski NA. Receiver operating characteristic curves and their use in radiology. Radiology 2003;229:3–8.

45. Obuchowski NA, Goske MJ, Applegate KE. Assessing physicians' accuracy in diagnosing paediatric patients with acute abdominal pain: measuring accuracy for multiple diseases. Stat Med 2001;20:3261–3278.

46. SAS Institute. SAS/STAT user's guide V. Cary, NC: SAS Institute, 2000.

47. Bossuyt PM, Reitsma JB, Bruns DE, et al. Towards complete and accurate reporting of studies of diagnostic accuracy: the STARD Initiative. Radiology 2003;226:24–28.

48. Seltzer SE, Getty DJ, Tempany CM, et al. Staging prostate cancer with MR imaging: a combined radiologist-computer system. Radiology 1997;202:219–226.

49. Mullerad M, Hricak H, Wang L, Chen HN, Kattan MW, Scardino PT. Prostate cancer: detection of extracapsular extension by genitourinary and general body radiologists at MR imaging. Radiology 2004;232:140–146.

50. Engelbrecht MR, Jager GJ, Laheij RJ, Verbeek AL, van Lier HJ, Barentsz JO. Local staging of prostate cancer using magnetic resonance imaging: a meta-analysis. Eur Radiol 2002;12:2294–2302.

51. Lovett K, Rifkin MD, McCue PA, Choi H. MR imaging characteristics of noncancerous lesions of the prostate. J Magn Reson Imaging 1992;2:35–39.

52. Schiebler ML, Tomaszewski JE, Bezzi M, et al. Prostatic carcinoma and benign prostatic hyperplasia: correlation of high-resolution MR and histopathologic findings. Radiology 1989;172:131–137.

53. Lencioni R, Menchi I, Paolicchi A, Carini M, Amorosi A, Bartolozzi C. Prediction of pathological tumor volume in clinically localized prostate cancer: value of endorectal coil magnetic resonance imaging. MAGMA 1997; 5:117–121.

54. Coakley FV, Kurhanewicz J, Lu Y, et al. Prostate cancer tumor volume: measurement with endorectal MR and MR spectroscopic imaging. Radiology 2002;223:91–97.

55. Schnall MD, Imai Y, Tomaszewski J, Pollack HM, Lenkinski RE, Kressel HY. Prostate cancer: local staging with endorectal surface coil MR imaging. Radiology 1991;178:797–802.

56. Sommer FG, Nghiem HV, Herfkens R, McNeal J, Low RN. Determining the volume of prostatic carcinoma: value of MR imaging with an external-array coil. AJR Am J Roentgenol 1993;161:81–86.

57. Furman-Haran E, Grobgeld D, Kelcz F, Degani H. Critical role of spatial resolution in dynamic contrast-enhanced breast MRI. J Magn Reson Imaging 2001;13:862–867.

58. Futterer JJ, Engelbrecht MR, Huisman HJ, et al. Staging prostate cancer with dynamic contrast-enhanced endorectal MR imaging prior to radical prostatectomy: experienced versus less experienced readers. Radiology 2005;237:541–549.

59. Futterer JJ, Heijmink SW, Scheenen TW, et al. Prostate cancer: local staging at 3-T endorectal MR imaging—early experience. Radiology 2006;238:184–191.

60. Rouviere O, Raudrant A, Ecochard R, et al. Characterization of time-enhancement curves of benign and malignant prostate tissue at dynamic MR imaging. Eur Radiol 2003;13:931–942.

61. Wang L, Mullerad M, Chen HN, et al. Prostate cancer: incremental value of endorectal MR imaging findings for prediction of extracapsular extension. Radiology 2004;232: 133–139.

62. Bloch BN, Rofsky NM, Baroni RH, Marquis RP, Pedrosa I, Lenkinski RE. 3 Tesla magnetic resonance imaging of the prostate with combined pelvic phased-array and endorectal coils: initial experience. Acad Radiol 2004;11:863–867.

63. Futterer JJ, Scheenen TW, Huisman HJ, et al. Initial experience of 3 tesla endorectal coil magnetic resonance imaging and 1H-spectroscopic imaging of the prostate. Invest Radiol 2004;39:671–680.